de Sitter space, extremal surfaces, and time entanglement

K. Narayan
Chennai Mathematical Institute, H1 SIPCOT IT Park, Siruseri 603103, India

(Received 8 November 2022; accepted 22 May 2023; published 9 June 2023)

We refine previous investigations on de Sitter space and extremal surfaces anchored at the future boundary I^+. Since such surfaces do not return, they require extra data or boundary conditions in the past (interior). In entirely Lorentzian de Sitter spacetime, this leads to future-past timelike surfaces stretching between $I^\pm$. Apart from an overall $-i$ factor (relative to spacelike surfaces in AdS) their areas are real and positive. With a no-boundary type boundary condition, the top half of these timelike surfaces joins with a spacelike part on the hemisphere giving a complex-valued area. Motivated by these, we describe two aspects of "time-entanglement" in simple toy models in quantum mechanics. One is based on a future-past thermofield double type state entangling timelike separated states, which leads to entirely positive structures. Another is based on the time evolution operator and reduced transition amplitudes, which leads to complex-valued entropy.

DOI: 10.1103/PhysRevD.107.126004

I. INTRODUCTION AND SUMMARY

It is of great interest to understand holography for de Sitter space (see the review [1]). In de Sitter (and cosmology more generally) perhaps the natural asymptotics are in the far future or the far past: this thinking leads to dS/CFT [2–4] (and [5] in the higher spin context), which associates a hypothetical nonunitary dual Euclidean CFT at the future boundary I^+, with several dramatic differences from AdS [6–8]. A particularly fascinating question is whether de Sitter entropy [9] can be understood as some sort of entanglement entropy. It is then natural to ask if the extensive investigations of holographic entanglement in AdS [10–12] can be generalized to de Sitter space.

One possible generalization of the Ryu-Takayanagi (RT) formulation to de Sitter space is to consider the bulk analog of setting up entanglement entropy in the dual Euclidean CFT on the future boundary [13]. We restrict to some boundary Euclidean time slice as a crutch, define subregions on these slices, and look for extremal surfaces anchored at I^+ dipping into the holographic (time) direction. Analyzing this extremization interestingly shows that surfaces anchored at I^+ do not return to I^+, i.e., there is no $I^+ \to I^+$ turning point, so there are no spacelike surfaces connecting points on I^+. There exist analytic continuations of RT surfaces in AdS which lead to complex extremal surfaces [13–16]. In [17,18], entirely timelike future-past extremal surfaces were studied, stretching from I^+ to I^-.

In this paper, we develop this further, stitching together an overall perspective which hopefully adds value to the understanding of these studies. The absence of $I^+ \to I^+$ returns for surfaces implies that surfaces starting at I^+ continue inward, to the past: this suggests that they require extra data or boundary conditions in the interior, or far past to be well defined. One obvious possibility for an entirely Lorentzian de Sitter space (Sec. II A) is that the surfaces then end at the past boundary I^-. Analyzing this in detail leads to future-past surfaces stated above [17,18]. These are timelike extremal surfaces stretching between subregions at I^+ and equivalent ones at I^-: they are akin to rotated analogs of the Hartman-Maldacena surfaces [19] in the eternal AdS black hole. Being entirely timelike, their area has an overall $-i$ factor, relative to the familiar spacelike extremal surfaces in AdS (this overall $-i$ was discarded in [17,18]; see below). Since we obtain codim-2 surfaces (when they exist), their area scales as de Sitter entropy.

Another possibility for the interior boundary conditions arises from modifying de Sitter from being entirely Lorentzian in accord with the Hartle-Hawking no-boundary prescription, i.e., to cut dS in the middle and remove the bottom half, replacing it with a hemisphere (Sec. II B). Now we join the top timelike part of the extremal surfaces above with regularity at the midslice to a spatial extremal surface that goes around the hemisphere (thus turning around): see [20,21] for dS_3. This spacelike part has real area so that the total area is complex valued. The top part of the surface (in the Lorentzian de Sitter) is the same as in the entirely timelike surfaces above: this reflects consistency of the future-past surfaces with Hartle-Hawking

boundary conditions. The finite real part of the area of the no-boundary surfaces arises from the hemisphere and is precisely half de Sitter entropy for any dimension when the subregion at I^+ becomes maximal. In Sec. IV, we give some comments on these future-past and no-boundary surface areas in terms of time contours, and argue that they can be regarded as space-time rotations from timelike subregions in AdS-like spaces.

Imaginary values also arise in studies of quantum extremal surfaces in de Sitter with regard to the future boundary [22,23], stemming from timelike separations (sec. II C). Complex-valued entanglement entropy was also found quite explicitly in studies of ghostlike theories, including simple toy quantum-mechanical models of "ghost spins," e.g. [24,25].

For entirely Lorentzian dS, the entirely timelike future-past surfaces are akin to entirely timelike geodesics for ordinary particles moving in time. Removing the overall $-i$ in their pure imaginary areas (relative to real spacelike surface areas) is akin to calling the length of timelike geodesics as "time" rather than "$-i\cdot$ space." Overall this suggests that the areas of these dS extremal surfaces with timelike components encode some new object, "time entanglement," distinct from usual spatial entanglement. In Sec. III, we describe two aspects of this in ordinary quantum mechanics, which incorporate this entry of late and early time boundary conditions. One is based on a future-past thermofield-double state [17] (see also [26,27]) which leads to entirely positive structures despite the timelike separation. The other involves the time-evolution operator and "reduced transition amplitudes," giving complex-valued entropy. As we were preparing this, the work [28] appeared with partial overlap.

II. dS EXTREMAL SURFACES FROM I^+, BOUNDARY CONDITIONS

The simplest place to see the absence of $I^+ \to I^+$ turning points [13] is in the Poincaré slicing with planar foliations, so

$$ds^2_{d+1} = \frac{R^2_{dS}}{\tau^2}(-d\tau^2 + dy_i^2) = \frac{R^2_{dS}}{\tau^2}(-d\tau^2 + dw^2 + dx_i^2). \tag{1}$$

Here we have singled out $w \in y_i$ as boundary Euclidean time, without loss of generality. Taking the $w=$ const slice, we consider at I^+ a strip-shaped subregion (the natural subregions consistent with planar symmetries), with width along $x \in x_i$ and extremal surfaces anchored from one boundary interface of the strip. This leads to the area functional and extremization,

$$S_{dS} = -i\frac{R^{d-1}_{dS}V_{d-2}}{4G_{d+1}}\int \frac{d\tau}{\tau^{d-1}}\sqrt{1-(\partial_\tau x)^2} \to (\partial_\tau x)^2 = \frac{B^2\tau^{2d-2}}{1+B^2\tau^{2d-2}}, \tag{2}$$

where B^2 is some constant. The fact that there is a minus sign relative to the extremization equation in AdS is the reflection of the absence of turning points back to I^+. We see that $(\partial_\tau x)^2 \ll 1$ near the boundary $\tau \sim 0$ and remains bounded with $(\partial_\tau x)^2 < 1$ throughout, for any real $B^2 > 0$. (The surfaces with $B^2 < 0$ are equivalent to analytic continuations from AdS RT surfaces [13–16].) We will return to this later.

The absence of $I^+ \to I^+$ return implies that the surfaces march on inward: this suggests they end at I^- if we focus on entirely Lorentzian de Sitter space. These lead to future-past extremal surfaces, timelike codim-2 surfaces stretching from I^+ to I^-. We describe this now, first in part reviewing the studies in [17,18]. Alternatively we could modify Lorentzian dS in accord with the Hartle-Hawking no-boundary prescription replacing the bottom half of dS by a hemisphere, and then impose a no-boundary type boundary condition on extremal surfaces. We will discuss these now.

A. Lorentzian dS

1. Static coordinates

These coordinates exhibit static patches exhibiting time translation symmetry, but allowing analytic extensions to the entire de Sitter space. We have

$$ds^2 = -\left(1-\frac{r^2}{l^2}\right)dt^2 + \frac{dr^2}{1-\frac{r^2}{l^2}} + r^2 d\Omega^2_{d-1}. \tag{3}$$

In the Northern/Southern diamond regions N/S, the static patches, t is time enjoying translation symmetry. Event horizons for observers in N/S are at $r=l$: the area of these cosmological horizons is de Sitter entropy. Towards studying the future boundary, we use $\tau = \frac{l}{r}$, $w = \frac{t}{l}$, to recast as $ds^2 = \frac{l^2}{\tau^2}(-\frac{d\tau^2}{1-\tau^2} + (1-\tau^2)dw^2 + d\Omega^2_{d-1})$: now τ is bulk time, with $\tau = 0$ the future/past boundary and the future/past universes described by $0 \le \tau < 1$. In this case the boundary at I^+ is $R \times S^{d-1}$. We can take the boundary Euclidean time slice as any S^{d-1} equatorial plane or as the $w=$ const slice.

Taking the boundary Euclidean time slice as some S^{d-1} equatorial plane, we define a subregion as $\Delta w \times S^{d-2} \in I^+$ and an equivalent one at I^-. Then we obtain the area functional $S = -i\frac{l^{d-1}V_{S^{d-2}}}{4G_{d+1}}\int \frac{d\tau}{\tau^{d-1}}\sqrt{\frac{1}{f}-f(w')^2}$ and extremization (with $B^2 > 0$ some constant)

$$(1-\tau^2)^2(w')^2 = \frac{B^2\tau^{2d-2}}{1-\tau^2+B^2\tau^{2d-2}}, \qquad S = -i\frac{2l^{d-1}V_{S^{d-2}}}{4G_{d+1}}\int_\epsilon^{\tau_*}\frac{d\tau}{\tau^{d-1}}\frac{1}{\sqrt{1-\tau^2+B^2\tau^{2d-2}}}. \tag{4}$$

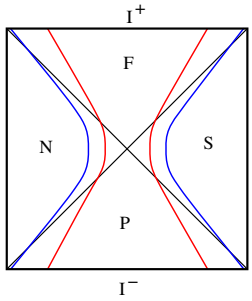

FIG. 1. dS future-past extremal surfaces stretching between $I^{\pm}$ on an S^{d-1} equatorial plane. The red curve is for a generic subregion while the blue curve is a limiting curve as the subregion becomes the whole space.

The factor of 2 in the area arises from considering both the top and bottom parts of the extremal surface (see Fig. 1, reproduced from [18]). There is now a real turning point τ_* at $1-\tau_*^2+B^2\tau_*^{2d-2}=0$, where $|\dot{w}|\to\infty$: this lies in the N/S diamond regions where the surface remains timelike. The surface from I^+ can be joined to an equivalent one from I^- (hence the factor of 2 in S above) which then gives the full, entirely timelike, future-past surface stretching from I^+ to I^-. These are rotated analogs of the Hartman-Maldacena surfaces in the eternal AdS black hole [19]. There is a limiting surface as $\Delta w\to\infty$ where the subregion becomes the whole space $I^{\pm}$. For dS_4 this occurs at $\tau_*=\sqrt{2}$ which corresponds to $B\to\frac{1}{2}$. These surfaces have an area law type divergence (always) and a finite part: for the limiting surface these are

$$S^{\rm div}\sim -i\frac{\pi l^2}{G_4}\frac{l}{\epsilon_c},\qquad S^{\rm fin}\sim -i\frac{\pi l^2}{G_4}\Delta w\quad [dS_4]. \tag{5}$$

It is not surprising that we obtain an overall scaling as de Sitter entropy $\frac{\pi l^2}{G_4}$, which is akin to the number of degrees of freedom in the dual CFT [recall that for an AdS_4 black hole the RT surface has area $S\sim\frac{R^2}{G_4}(\frac{V}{\epsilon}+\#T^2Vl)$]. These future-past surfaces exhibit various features [18]: e.g. the absence of $I^+\to I^+$ returns implies that mutual information vanishes.

Considering the $w=$ const slice as the boundary Euclidean time slice, we consider cap-like subregions defined by $\theta=$ const latitudes on S^{d-1} at I^+ and equivalent ones at I^-. Then

$$S=-i\frac{2l^{d-1}V_{S^{d-2}}}{4G_{d+1}}\int\frac{d\tau}{\tau^{d-1}}(\sin\theta)^{d-2}\sqrt{\frac{1}{1-\tau^2}-(\theta')^2} \tag{6}$$

which is difficult to analyze explicitly for caps at generic θ. However, at $\theta=\frac{\pi}{2}$ it is straightforward to see that we obtain a future-past extremal surface from the hemispherical cap on $S^{d-1}\in I^+$ to the corresponding one at I^- [17]. This gives area

$$S=-i\frac{2l^{d-1}V_{S^{d-2}}}{4G_{d+1}}\int_\epsilon^1\frac{d\tau}{\tau^{d-1}}\frac{1}{\sqrt{1-\tau^2}}\xrightarrow{dS_4}-i\frac{\pi l^2}{G_4}\frac{1}{\epsilon} \tag{7}$$

with no finite part.

2. Global

Here we have sphere foliations with

$$ds^2_{d+1}=-d\tau^2+l^2\cosh^2\frac{\tau}{l}d\Omega_d^2 \tag{8}$$

and we can take the boundary Euclidean time slice to be any S^d equatorial plane (which are all equivalent). Then we obtain the area functional (with factor of 2 for top + bottom)

$$S=-i\frac{2l^{d-2}V_{S^{d-2}}}{4G_{d+1}}\int d\tau(\cosh\tau)^{d-2}(\sin\theta)^{d-2}\times\sqrt{1-\cosh^2\tau(\partial_\tau\theta)^2} \tag{9}$$

which has structural similarities to the $w=$ const slice above. At $\theta=\frac{\pi}{2}$ it is straightforward to see a future-past extremal surface stretching from I^+ to I^- with area (focusing on dS_4)

$$S=-i\frac{\pi l^2}{G_4}\int_0^{\tau_c/l}d\tau\,\cosh\tau\sim -i\frac{\pi l^2}{2G_4}e^{\tau_c/l}\sim -i\frac{\pi l^2}{2G_4}\frac{l}{T_c}. \tag{10}$$

This is an area law divergence type term, with no finite part. The last expression has been obtained by noting that near I^+ we have $ds^2=-d\tau^2+l^2e^{2\tau/l}d\Omega_3^2\sim\frac{l^2}{T^2}(-dT^2+l^2d\Omega_3^2)$, with cutoff $T_c=le^{-\tau_c/l}\sim 0$ near $\tau_c\to\infty$. The area law divergence is structurally similar to the static coordinates case earlier.

3. Poincaré

The full de Sitter space is obtained from two Poincaré patches joined at the past horizon $\tau\to-\infty$. Now based on the above descriptions for the static and global coordinate systems, we can likewise construct future-past surfaces by imposing regularity boundary conditions on the past horizon. For the surface stretching down from I^+ described by the extremization (2), we require that the derivatives $\partial_\tau x$ match smoothly onto the corresponding ones for a corresponding surface stretching up from I^-. Note that $(\partial_\tau x)^2\to 1$ as $\tau\to-\infty$. The detailed continuation is similar to that in [17,18] for the static coordinates. This leads to just the area law term again, giving $S_{dS_4}\sim -i\frac{2l^2}{4G_4}\frac{V}{\epsilon}$.

B. dS no-boundary surfaces

In accord with the Hartle-Hawking no-boundary prescription [29] (see also [30]), let us cut global de Sitter

space in the middle, on the $\tau = 0$ time slice and join the top half with a hemisphere in the bottom half: this hemisphere is given by the Euclidean continuation

$$ds^2 = l^2 d\tau_E^2 + l^2 \cos^2\tau_E d\Omega_d^2; \quad \tau = il\tau_E, \quad 0 \le \tau_E \le \frac{\pi}{2}. \tag{11}$$

Consider now some S^d equatorial plane (i.e., S^{d-1}) and the timelike extremal surface in (9), at $\theta = \frac{\pi}{2}$ which is the IR limit of such surfaces. The top part of this surface from I^+ hits the $\tau = 0$ midslice "vertically": we join this smoothly at $\tau = 0$ with a surface that goes around the bottom hemisphere, Fig. 3 (see [20] for dS_3). This joining being smooth implies consistency with the Hartle-Hawking prescription. This IR surface is

$$\begin{aligned} ds^2 &= l^2 d\tau_E^2 + l^2 \cos^2\tau_E (d\theta^2 + \sin^2\theta d\Omega_{d-2}^2))|_{\theta=\frac{\pi}{2}} \\ &= l^2 d\tau_E^2 + l^2 \cos^2\tau_E d\Omega_{d-2}^2 \end{aligned}$$

and gives area

$$\begin{aligned} &\frac{l^{d-1}}{4G_{d+1}} V_{S^{d-2}} \int_0^{\pi/2} d\tau_E (\cos\tau_E)^{d-2} \\ &\quad = \frac{l^{d-1}}{4G_{d+1}} V_{S^{d-2}} \frac{\sqrt{\pi}\Gamma(\frac{d-1}{2})}{2\Gamma(\frac{d}{2})} = \frac{1}{2}\frac{l^{d-1} V_{S^{d-1}}}{4G_{d+1}}, \end{aligned} \tag{12}$$

using the expression $V_{S^d} = \frac{2\pi^{(d+1)/2}}{\Gamma((d+1)/2)}$ for a d sphere. This real part of the area of this spacelike surface on the hemisphere is precisely half of de Sitter entropy. This recovery of the entropy is in detail somewhat different from the realization of de Sitter entropy as the area of the cosmological horizon from the point of view of static patch observers. In particular, one of the hemisphere directions that enters here is the Euclidean continuation of the time direction in the future universe.

Focusing on dS_4, the full area for this no-boundary surface is the sum of the top timelike part (which is half of the future-past area (10)) and the hemisphere part becomes

$$S = -i\frac{\pi l^2}{4G_4}\frac{l}{T_c} + \frac{\pi l^2}{2G_4}. \tag{13}$$

There are some similarities between these no-boundary surface areas and the semiclassical Wavefunction $\Psi_{dS} = e^{iS_{cl}}$ for no-boundary dS_4, with S_{cl} the action. The top Lorentzian half has real S_{cl} which gives a pure phase in Ψ_{dS}. The bottom hemisphere arises after the continuation (11) to Euclidean time (the no-boundary point is $\tau_E = \frac{\pi}{2}$ here): iS_{cl} continues to the Euclidean gravity action $-\int_{nbp}\sqrt{g}(R - 2\Lambda)$ pertaining to the hemisphere, which for dS_4 gives $\frac{1}{2}\frac{l^4 V_{S^4}}{16\pi G_4}\frac{6}{l^2} = \frac{\pi l^2}{2G_4}$ as is well known (see e.g. [31,32]).

A similar calculation of the spatial surface on the hemisphere can be done for the timelike future-past surface in the static coordinates discussed earlier. In this case, the boundary was $R_w \times S^{d-1}$ leading to either any S^{d-1} equatorial plane or the $w = $ const slice as the boundary Euclidean time slice. The Euclidean continuation in this case is

$$\begin{aligned} &ds^2 = l^2(\cos^2\psi d\tau_E^2 + d\psi^2 + \sin^2\psi d\Omega_{d-1}^2), \qquad t = i\tau_E, \\ &r = l\sin\psi, \end{aligned} \tag{14}$$

where $\tau_E \in [0, 2\pi l]$ and $0 \le \psi \le \frac{\pi}{2}$. First, considering the S^{d-1} equatorial plane surfaces, we saw that there is a limiting surface at $\tau_* > 1$ (this is $\tau_* = \sqrt{2}$ for dS_4) which translates to some limiting value ψ_* given by $\sin\psi_* = \frac{r_*}{l} = \frac{1}{\tau_*}$. Then the surface is described by

$$\begin{aligned} ds^2 &= \cos^2\psi_* d\tau_E^2 + \sin^2\psi_* d\Omega_{d-2}^2 \to \text{Area} \\ &= \int_0^{\pi l} \cos\psi_* d\tau_E (\sin\psi_*)^{d-2} V_{S^{d-2}} \frac{l^{d-2}}{4G_{d+1}}. \end{aligned} \tag{15}$$

Focusing on dS_4 we have $\sin\psi_* = \frac{1}{\tau_*} = \frac{1}{\sqrt{2}}$ giving the area $\frac{1}{2}(\pi l)\frac{2\pi l}{4G_4} = \frac{\pi^2 l^2}{4G_4}$. This apparently unrecognizable value is perhaps not surprising due to the limiting surface.

For the $w = $ const slice (equivalently $\tau_E = $ const), the timelike surface from the $\theta = \frac{\pi}{2}$ cap on S^{d-1} leads on the hemisphere to

$$\begin{aligned} ds^2 &= d\psi^2 + \sin\psi^2 d\Omega_{d-2}^2 \to \text{Area} \\ &= \frac{l^{d-1} V_{S^{d-2}}}{4G_{d+1}} \int_0^{\pi/2} d\psi (\sin\psi)^{d-2} = \frac{1}{2}\frac{l^{d-1} V_{S^{d-1}}}{4G_{d+1}}, \end{aligned} \tag{16}$$

identical to global dS (12) above, not surprising given the similarities in the calculation for this slice. With the top timelike part from (7), the total area becomes $S = -i\frac{\pi l^2}{2G_4}\frac{1}{\epsilon} + \frac{\pi l^2}{2G_4}$ for dS_4.

Note that all these no-boundary surfaces turn around only in the bottom hemisphere: the top timelike half is identical to the corresponding future-past surface and there is no $I^+ \to I^+$ turning point there. Thus, if we consider two disjoint subregions the corresponding no-boundary surfaces are unique (following from the top halves of the corresponding future-past surfaces), with no new connected surface emerging: so $S[A \cup B] = S[A] + S[B]$. Thus, as for the future-past surfaces [18], mutual information vanishes here as well.

C. 2-dim CFT, timelike subsystems, complex EE

Now consider dS_3, special for various reasons. In entirely Lorentzian global de Sitter, the future-past surfaces on some S^2 equatorial plane slice (9) give area $S = -i\frac{l}{G_3}\log\frac{l}{T_c}$. If we consider no-boundary dS_3, the total

area from the top timelike part and the hemisphere part (12) becomes

$$S_{dS_3} = -i\frac{l}{2G_3}\log\frac{l}{T_c} + \frac{\pi l}{4G_3}. \tag{17}$$

The last (real) term is half dS_3 entropy $\frac{\pi l}{2G_3}$. The whole expression can be seen to be an overall $-i$ times the familiar $\frac{c}{6}\log\frac{L^2}{\epsilon^2}$ [33–35] with $c = \frac{3l_{AdS}}{2G}$ the AdS_3 central charge, along with $\frac{l^2}{T_c^2} \to -\frac{l^2}{T_c^2}$ [so $\log(-1) = i\pi$]. Note that dS_3/CFT_2 has $c_{dS_3} = -i\frac{3l_{dS}}{2G}$ [4] which for single intervals would give imaginary S as for the entirely Lorentzian future-past surfaces stated above. So perhaps what is most striking in (17) is the real part arising from the hemisphere which then requires an additional i, which is a novel feature of this Euclidean CFT_{dS_3} dual (in contrast with ordinary Euclidean CFTs with simply real spatial lengths and no time). Further related comments appear in Sec. IV.

To put this in perspective, for ordinary unitary 2-dim CFTs, the entanglement entropy is

$$S = \frac{c}{6}\log\frac{\Delta^2}{\epsilon^2} = \frac{c}{6}\log\frac{-(\Delta t)^2 + (\Delta x)^2}{\epsilon^2}. \tag{18}$$

For ordinary spacelike intervals Δ^2, we obtain the familiar $S = \frac{c}{3}\log\frac{\Delta x}{\epsilon}$. On the other hand, suppose we rotate the subsystem to be entirely timelike with some width Δt in the time direction. This gives

$$S = \frac{c}{3}\log\frac{\Delta t}{\epsilon} + \frac{c}{6}(i\pi), \tag{19}$$

the imaginary part arising from $\log(-1)$ in the timelike separation in the interval (more generally the real part contains $\Delta^2 < 0$). This imaginary part has appeared previously in studies of quantum extremal surfaces in de Sitter with regard to the future boundary [22,23]. The bulk matter is modeled as a 2-dim CFT with some central charge $c > 0$ but the timelike separation of the quantum extremal surface gives $\Delta^2 < 0$ in (18) above.

The usual replica formulation of entanglement entropy for a single interval proceeds by picking the interval $\Delta x \equiv [u, v]$ on some Euclidean time slice $\tau_E = \text{const}$, then constructing n replica copies glued at the interval end points. Evaluating $\text{Tr}\rho_A^n$ can be mapped to the twist operator two-point function which then leads finally to the entanglement entropy $S_A = -\lim_{n\to 1}\partial_n \text{Tr}\rho_A^n$. The only data here is the CFT central charge and the interval in question. The above Euclidean formulation applies for a timelike interval as well, with the only change being that the Euclidean time slice is $x = \text{const}$ and the interval is $\Delta t \equiv [u_t, v_t]$. However, in continuing back to Lorentzian time, we rotate u_t, v_t, to $-iu_t, -iv_t$, and so we obtain $\Delta^2 = -(v_t - u_t)^2 = -(\Delta t)^2$, which gives (19) above. This of course requires that the CFT contains some time direction.

It is also worth noting that complex-valued entanglement entropy arises quite explicitly in studies of ghostlike theories and simple quantum mechanical toy models of "ghost spins" [24,25]: in this case the reduced density matrix acquires minus signs due to contributions from negative norm states. Defining contractions over the ghost-spin Hilbert space appropriately leads to consistent expressions for the reduced density matrix and entanglement entropy, which are in general complex valued.

III. "TIME ENTANGLEMENT" IN QUANTUM MECHANICS

We have constructed future-past extremal surfaces stretching from I^+ to I^-. Since they are entirely timelike, their area is pure imaginary, with an overall $-i$ relative to the area of the familiar spacelike RT/HRT surfaces in AdS. However, apart from this overall $-i$, the area is real and positive: the overall $-i$ is a uniform factor, for any subregion at I^+. This is a bit reminiscent of the length of timelike geodesics having an overall $-i$ relative to the length of spacelike geodesics. We call this timelike length as "time" rather than "$-i\cdot$ space". This suggests that the areas of the entirely timelike future-past extremal surfaces encode some new object, "time entanglement".

Recall now the appearance of complex-valued areas for the no-boundary surfaces which are closely related to the entirely timelike future-past surfaces: they comprise a timelike component which is identical to the top half of the future-past one and a spacelike component from the hemisphere glued in the bottom half. The area is now complex, with a pure imaginary part from the top timelike component and a real part from the hemisphere component.

We now describe two aspects of this notion of time entanglement in quantum mechanics (independent of de Sitter at this point). The first is based on the thermofield-double type state described in [17,18], while the second is based on the time-evolution operator, regarding the timelike surfaces as some sort of transition amplitude.

A. A future-past thermofield double state

The entirely timelike future-past surfaces, akin to rotated Hartman-Maldacena surfaces [19], suggest some sort of entanglement between $I^{\pm}$, so consider

$$|\psi\rangle_{fp} = \sum \psi^{i_n^F, i_n^P} |i_n\rangle_F |i_n\rangle_P. \tag{20}$$

This was written down in [17] as an entirely positive object entangling identical F and P components (with intuition based on the thermofield double (TFD) state for the eternal black hole [36]). A partial trace over the second (P) copy gives a reduced density matrix with nontrivial entanglement entropy. To see how this works, let us consider a very

simple toy example of a two-state system in ordinary quantum mechanics. The action of the Hamiltonian H on these (orthogonal basis) eigenstates and the resulting (simple) time evolution are

$$H|k\rangle = E_k|k\rangle, \quad k = 1,2; \qquad |k\rangle_F \equiv |k(t)\rangle = e^{-iE_k t}|k\rangle_P, \quad [\langle 1|2\rangle = 0]. \tag{21}$$

We consider the F and P slices to be separated by time t and obtain the F state from the P state by time evolution through t. The future-past TFD state (20) in this toy case is

$$|\psi\rangle_{fp} = \frac{1}{\sqrt{2}}|1\rangle_F|1\rangle_P + \frac{1}{\sqrt{2}}|2\rangle_F|2\rangle_P = \frac{1}{\sqrt{2}}e^{-iE_1 t}|1\rangle_P|1\rangle_P + \frac{1}{\sqrt{2}}e^{-iE_2 t}|2\rangle_P|2\rangle_P. \tag{22}$$

We have normalized the coefficients for maximal entanglement at $t = 0$. For nonzero t, there are extra phases due to the time evolution but they cancel in the reduced density matrix obtained by tracing $|\psi\rangle_{fp}\langle\psi|_{fp}$ over the entire second copy as $\delta_{ij}\psi^{ki}_{fp}(\psi^*_{fp})^{lj}$, so

$$\rho_{fp} = \mathrm{Tr}_P|\psi\rangle_{fp}\langle\psi|_{fp} = \frac{1}{2}|1\rangle_F\langle 1|_F + \frac{1}{2}|2\rangle_F\langle 2|_F. \tag{23}$$

Now imagine a two-spin analogy, with $|1\rangle = |++\rangle$, $|2\rangle = |--\rangle$, i.e., we identify $1\rangle, |2\rangle$ with the two-state subspace $|\pm\pm\rangle$ of two spins with states $|\pm\rangle$ each for simplicity and concreteness. Then a partial trace over the second component gives the reduced density matrix $Tr_2\rho_{fp} = \frac{1}{2}|+\rangle_F\langle +|_F + \frac{1}{2}|-\rangle_F\langle -|_F$ again with an entirely positive structure, and entropy log 2.

If the states in question are not ordinary spins but ghost spins with negative norm states, as discussed in [17] based on the studies in [24,25], the fact that we have entangled identical components in both the future and past copies ensures that the minus signs cancel in $\gamma_{\sigma\rho}\psi^{\alpha\sigma}_{fp}(\psi^*_{fp})^{\beta\rho}$ (with γ_{ij} the indefinite ghost-spin metric) again yielding an entirely positive structure.

This future-past TFD state with timelike separation is quite different in principle from the usual TFD state. This positive structure despite the timelike separation is in some sense similar in spirit to the areas of the entirely timelike surfaces after stripping off the universal overall $-i$.

B. Time-evolution and reduced transition amplitudes

Unlike AdS where specifying boundary data fixes the extremization problem, dS extremal surfaces starting at late times on I^+ do not return, thus requiring extra data on boundary conditions in the far past. This is reminiscent of scattering amplitudes, i.e., final states from initial states, or equivalently time evolution. It is then amusing to ask for entanglement-like structures arising from the time evolution operator $\mathcal{U}(t)$ after a partial trace over some environment: in other words, we look for a "reduced transition amplitude" and its entropy. This suggests (taking A subregion, B environment)

$$\rho_t(t) \equiv \frac{\mathcal{U}(t)}{\mathrm{Tr}\mathcal{U}(0)} \to \rho^A_t = tr_B\rho_t \to S_A = -tr(\rho^A_t \log \rho^A_t). \tag{24}$$

The normalization is so we obtain ordinary entanglement structures at $t = 0$, as we will see explicitly. To illustrate, consider again the very simple toy example (21) above. Since everything is diagonal here, the normalized time evolution operator is simple, becoming

$$\mathcal{U}(t) = e^{-iHt}: \ \rho_t(t) = \frac{1}{2}e^{-iE_1 t}|1\rangle_P\langle 1|_P + \frac{1}{2}e^{-iE_2 t}|2\rangle_P\langle 2|_P = \frac{1}{2}|1\rangle_F\langle 1|_P + \frac{1}{2}|2\rangle_F\langle 2|_P. \tag{25}$$

Now recall the two-spin analogy: $|1\rangle = |++\rangle$, $|2\rangle = |--\rangle$. A partial trace over the second components gives

$$\rho^A_t = \frac{1}{2}e^{-iE_1 t}|+\rangle_P\langle +|_P + \frac{1}{2}e^{-iE_2 t}|-\rangle_P\langle -|_P, \tag{26}$$

$$S_A = -\sum_i \frac{1}{2}e^{-iE_i t}\log\left(\frac{1}{2}e^{-iE_i t}\right) = \frac{1}{2}\log 2(e^{-iE_1 t} + e^{-iE_2 t}) + \frac{1}{2}(iE_1 t)e^{-iE_1 t} + \frac{1}{2}(iE_2 t)e^{-iE_2 t}. \tag{27}$$

Normalizing $\mathcal{U}(t)$ by its trace at time t gives $\mathrm{Tr}\rho_t(t) = 1$ for all t (not just $t = 0$), modifying (24)–(27) to

$$\rho_t(t) \equiv \frac{\mathcal{U}(t)}{\mathrm{Tr}\mathcal{U}(t)} \Rightarrow \rho_t(t) = \sum_i p_i|i\rangle_P\langle i|_P, \quad p_i = \frac{e^{-iE_i t}}{\sum_j e^{-iE_j t}}, \to \rho^A_t = \sum_i p'_i|i'\rangle_P\langle i'|_P \to S_A = -\sum_i p'_i \log p'_i, \tag{28}$$

where $H|i\rangle = E_i|i\rangle$ and the second line arises after partial trace. There are similarities with pseudo-entropy [37] although the details above look different *a priori*. There are close interrelations between time entanglement above (entanglement-like structures based on the time evolution operator regarded as a density operator) and pseudo-entropy: some of these explorations in quantum mechanics with various interesting new features appear in [38], which also elaborates on some results outlined below.

ρ^A_t resembles an ordinary maximally entangled state at $t = 0$. Any later time $t \neq 0$ gives complex-valued entropy in general (although there are real subfamilies: e.g. (28) for the two-state case contains a single phase $e^{-i(E_2-E_1)t}$ and gives S_A real). Further the different normalizations give different results in detail, as is already clear in the simple cases above. Overall these structures resemble the usual

finite temperature mixed state entanglement, except with imaginary temperature, i.e., $\beta = it$.

There are also related quantities that arise along similar lines. For instance, the time evolution operator $\mathcal{U}(t)$ along with a projection operator onto a generic state $|I\rangle$ gives $\mathcal{U}(t)|I\rangle\langle I| = |F_I(t)\rangle\langle I|$, where $|F_I(t)\rangle$ is the future state time evolved from the initial state $|I\rangle$. Normalizing at time t and performing a partial trace gives a reduced transition matrix which resembles that in pseudo-entropy [37] but with the future state specifically corresponding to the time evolved state. Relatedly, normalizing at $t = 0$ gives different structures. For instance, projection onto Hamiltonian eigenstates $|E_I\rangle$ and performing partial trace gives simple phases for $\rho_t^{A,I}$ [essentially components of (26)], so the corresponding entropy (27) is of the form, e.g., $iE_I te^{-iE_I t}$.

IV. DISCUSSION: dS SURFACES, TIME CONTOURS, ROTATIONS

We have seen that the absence of $I^+ \to I^+$ turning points for dS extremal surfaces anchored at the future boundary leads to either future-past surfaces or no-boundary surfaces. Since these surfaces are characterized by area integrals which ultimately reduce to simple integrals over the time direction, they can be organized and recast in terms of time contours, which leads to certain clarifications. Towards this, recall that the future-past and no-boundary surface areas [(9) and (12)] are of the schematic form (with a reduced area functional $a(\tau)$)

$$S_{fp} \sim 2 \cdot -iS_0 \int_{\tau_{cF}}^{\tau_*} d\tau a(\tau), \qquad [\tau\colon \tau_{cF} \to \tau_* \to \tau_{cP}];$$
$$S_{nb} \sim -iS_0 \int_{\tau_{cF}}^{\tau_*} d\tau a(\tau) + S_0 \int_{\tau_{E*}}^{nbp} d\tau_E a_E(\tau_E),$$
$$[\tau\colon \tau_{cF} \to \tau_* \to nbp], \tag{29}$$

where S_0 is de Sitter entropy, τ_{cF} labels the anchoring cutoff slice at I^+ and τ_* is the bulk point where the surface is going "vertically down" (Figs. 2 and 3). nbp refers to the no-boundary point. In the no-boundary surfaces, the time contour goes along the real time direction until τ_* and then

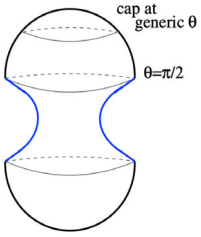

FIG. 2. Global dS future-past extremal surfaces stretching between $I^{\pm}$ on any S^d equatorial plane in the IR limit ($\theta = \frac{\pi}{2}$). This is also the picture for the $w =$ const slice in the static coordinates.

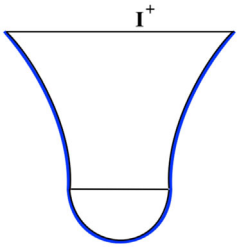

FIG. 3. Global dS no-boundary extremal surfaces, with a top timelike part joining smoothly with a spatial part going around the hemisphere in the bottom half. The blue curve is the IR limit ($\theta = \frac{\pi}{2}$) on some S^d equatorial plane. This is also the picture for the $w =$ const slice in the static coordinates.

along the Euclidean time path until the nbp. As we saw, these simplify in the IR limit to give

$$S_{fp} = -2iS_0 I[\tau_{cF}, \tau_*]; \qquad S_{nb} = -iS_0 I[\tau_{cF}, \tau_*] + \frac{S_0}{2};$$
$$\Rightarrow S_{fp} = S_{nb} - S_{nb}^*. \tag{30}$$

In this light, it is reasonable to think that the future-past surface is made of two copies of the no-boundary surface, but with the time contour schematically being $[\tau_{cF} \to \tau_* \to \tau_{cP}] = [\tau_{cF} \to \tau_* \to nbp] + [nbp \to \tau_* \to \tau_{cP}]$. Then the real parts in the two copies of S_{nb} cancel to give a pure imaginary S_{fp}. Regarding S_{nb} as some time entanglement entropy arising from one dual boundary Euclidean CFT copy $Z_{CFT} = \Psi_{dS}$ via dS/CFT [2–4] suggests regarding S_{fp} as arising from two copies $\Psi_{dS}^*\Psi_{dS}$. It would be interesting to flesh this out more precisely from a replica formulation, perhaps developing [39] here.

Looking now at the expressions in detail for dS_3 and dS_4, i.e., (17), (10), and (13), we have

$$dS_3\colon xS_{fp} = -i\frac{l}{G_3}\log\frac{l}{\epsilon}; \quad S_{nb} = -i\frac{l}{2G_3}\log\frac{l}{\epsilon} + \frac{l}{2G_3}\frac{\pi}{2}.$$
$$dS_4\colon S_{fp} = -i\frac{\pi l^2}{2G_4}\frac{l}{\epsilon}; \quad S_{nb} = -i\frac{\pi l^2}{4G_4}\frac{l}{\epsilon} + \frac{\pi l^2}{2G_4}, \tag{31}$$

with $\epsilon \equiv T_c$ in the dS_4 expressions (10) and (13). For dS_5 there are pure imaginary subleading divergent terms as well, from the timelike I integral in (30). Writing the dS_3 expression as

$$dS_3 : S_{nb} = -i\left(\frac{c}{3}\log\frac{l}{\epsilon} + \frac{c}{6}(i\pi)\right), \qquad c = \frac{3l}{2G_3}, \tag{32}$$

suggests that these no-boundary surfaces are a rotation from some surfaces in AdS_3, with central charge $c_{AdS_3} = c$ (recall that the dS_3/CFT_2 central charge is $c_{dS_3} = -ic$): specifically the overall $-i$ arises from the AdS_3 radial integral reinterpreted as a time integral in dS_3. The term inside the brackets is essentially the entanglement

entropy (19) for a timelike interval in 2-dim CFT: the real logarithmic part is a spatial area contribution in AdS_3, while the imaginary part is a timelike contribution. Thus the real spacelike part of the dS_3 surface, from the Euclidean hemisphere, maps to a pure imaginary, timelike, contribution in AdS_3.

The dS_4 case (13) can be similarly recast as

$$dS_4:\ S_{nb} = -i\left(\frac{\pi l^2}{4G_4}\frac{l}{\epsilon} + i\frac{\pi l^2}{2G_4}\right), \qquad S_0 = \frac{\pi l^2}{G_4}, \quad (33)$$

which again resembles an overall rotation from an AdS_4 surface, encoded by the overall $-i$. Again, the term inside has a real part corresponding to half of the Hartman-Maldacena-like spacelike surface contribution while the imaginary part is a timelike contribution. The fact that all de Sitter no-boundary surfaces have area of the form (30), i.e.,

$$S_{nb} = -i\left(S_0 I + i\frac{S_0}{2}\right), \quad (34)$$

suggests that the surfaces can be regarded as space-time rotations from timelike subregions in AdS-like spaces. In general, these are distinct from analytic continuations of Poincaré AdS RT expressions, which correspond to distinct time contours (along imaginary time paths) [13–15]: e.g. in dS_4 those give real negative area. However, these can be mapped to other appropriate analytic continuations from AdS (see [28]).

Note that this is consistent with the dS future-past surfaces (see Fig. 1) being akin to space-time rotations of Hartman-Maldacena surfaces in the AdS black hole [19], as discussed in [17,18]. In that case, the dS area S_{fp} is pure imaginary, with the overall $-i$ encoding the rotation from a real spacelike area in AdS.

The pure imaginary part of the no-boundary dS_3 surface area can be identified with $\frac{c}{3}\ \log\ \frac{l}{\epsilon}$ for a half-size interval in a Euclidean CFT on a circle [34]: the future-past surfaces have twice this area, and so correspond to two copies. The real spacelike part of the no-boundary area, arising from a deep interior Euclideanization of de Sitter, presumably indicates some new IR aspect of the dual Euclidean CFT that encodes "interior regularity."

There are some parallels in the thinking in Sec. III via the time evolution operator and viewing de Sitter space as a collection of past-future amplitudes [3]. This suggests using the S-matrix $|f\rangle\langle i|$ with initial and final states appropriate to dS to analyze entanglement-like structures. Needless to say, there are many things to explore here, in quantum mechanics, de Sitter holography and time.

ACKNOWLEDGMENTS

It is a pleasure to thank Abhijit Gadde, Alok Laddha, Shiraz Minwalla and Sandip Trivedi for helpful discussions. I also thank Tadashi Takayanagi for conversations on the overall $-i$ following [17], which have influenced my thinking. This work is partially supported by a grant to CMI from the Infosys Foundation.

[1] M. Spradlin, A. Strominger, and A. Volovich, Les Houches lectures on de Sitter space, arXiv:hep-th/0110007.
[2] A. Strominger, The dS/CFT correspondence, J. High Energy Phys. 10 (2001) 034.
[3] E. Witten, Quantum gravity in de Sitter space, arXiv:hep-th/0106109.
[4] J. M. Maldacena, Non-Gaussian features of primordial fluctuations in single field inflationary models, J. High Energy Phys. 05 (2003) 013.
[5] D. Anninos, T. Hartman, and A. Strominger, Higher spin realization of the dS/CFT correspondence, Classical Quantum Gravity **34**, 015009 (2017).
[6] J. M. Maldacena, The large N limit of superconformal field theories and supergravity, Adv. Theor. Math. Phys. **2**, 231 (1998); [Int. J. Theor. Phys. **38**, 1113 (1999)].
[7] S. S. Gubser, I. R. Klebanov, and A. M. Polyakov, Gauge theory correlators from non-critical string theory, Phys. Lett. B **428**, 105 (1998).
[8] E. Witten, Anti-de Sitter space and holography, Adv. Theor. Math. Phys. **2**, 253 (1998).
[9] G. W. Gibbons and S. W. Hawking, Cosmological event horizons, thermodynamics, and particle creation, Phys. Rev. D **15**, 2738 (1977).
[10] S. Ryu and T. Takayanagi, Holographic Derivation of Entanglement Entropy from AdS/CFT, Phys. Rev. Lett. **96**, 181602 (2006).
[11] S. Ryu and T. Takayanagi, Aspects of holographic entanglement entropy, J. High Energy Phys. 08 (2006) 045.
[12] V. E. Hubeny, M. Rangamani, and T. Takayanagi, A covariant holographic entanglement entropy proposal, J. High Energy Phys. 07 (2007) 062.
[13] K. Narayan, de Sitter extremal surfaces, Phys. Rev. D **91**, 126011 (2015).
[14] K. Narayan, De Sitter space and extremal surfaces for spheres, Phys. Lett. B **753**, 308 (2016).
[15] Y. Sato, Comments on entanglement entropy in the dS/CFT correspondence, Phys. Rev. D **91**, 086009 (2015).
[16] M. Miyaji and T. Takayanagi, Surface/state correspondence as a generalized holography, Prog. Theor. Exp. Phys. **2015**, 073B03 (2015).

[17] K. Narayan, On extremal surfaces and de Sitter entropy, Phys. Lett. B **779**, 214 (2018).
[18] K. Narayan, De Sitter future-past extremal surfaces and the entanglement wedge, Phys. Rev. D **101**, 086014 (2020).
[19] T. Hartman and J. Maldacena, Time evolution of entanglement entropy from black hole interiors, J. High Energy Phys. 05 (2013) 014.
[20] Y. Hikida, T. Nishioka, T. Takayanagi, and Y. Taki, CFT duals of three-dimensional de Sitter gravity, J. High Energy Phys. 05 (2022) 129.
[21] Y. Hikida, T. Nishioka, T. Takayanagi, and Y. Taki, Holography in de Sitter space via Chern-Simons gauge theory, Phys. Rev. Lett. **129**, 041601 (2022).
[22] Y. Chen, V. Gorbenko, and J. Maldacena, Bra-ket wormholes in gravitationally prepared states, J. High Energy Phys. 02 (2021) 009.
[23] K. Goswami, K. Narayan, and H. K. Saini, Cosmologies, singularities and quantum extremal surfaces, J. High Energy Phys. 03 (2022) 201.
[24] K. Narayan, On dS_4 extremal surfaces and entanglement entropy in some ghost CFTs, Phys. Rev. D **94**, 046001 (2016).
[25] D. P. Jatkar and K. Narayan, Ghost-spin chains, entanglement and bc-ghost CFTs, Phys. Rev. D **96**, 106015 (2017).
[26] C. Arias, F. Diaz, and P. Sundell, De Sitter space and entanglement, Classical Quantum Gravity **37**, 015009 (2020).
[27] C. Arias, F. Diaz, R. Olea, and P. Sundell, Liouville description of conical defects in dS_4, Gibbons-Hawking entropy as modular entropy, and dS_3 holography, J. High Energy Phys. 04 (2020) 124.
[28] K. Doi, J. Harper, A. Mollabashi, T. Takayanagi, and Y. Taki, Pseudo Entropy in dS/CFT and Time-like Entanglement Entropy, Phys. Rev. Lett. **130**, 031601 (2023).
[29] J. B. Hartle and S. W. Hawking, Wave function of the universe, Phys. Rev. D **28**, 2960 (1983).
[30] J. Maldacena, G. J. Turiaci, and Z. Yang, Two dimensional nearly de Sitter gravity, J. High Energy Phys. 01 (2021) 139.
[31] R. Bousso and S. W. Hawking, The probability for primordial black holes, Phys. Rev. D **52**, 5659 (1995).
[32] R. Bousso and S. W. Hawking, Pair creation of black holes during inflation, Phys. Rev. D **54**, 6312 (1996).
[33] C. Holzhey, F. Larsen, and F. Wilczek, Geometric and renormalized entropy in conformal field theory, Nucl. Phys. **B424**, 443 (1994).
[34] P. Calabrese and J. L. Cardy, Entanglement entropy and quantum field theory, J. Stat. Mech. (2004) P06002.
[35] P. Calabrese and J. Cardy, Entanglement entropy and conformal field theory, J. Phys. A **42**, 504005 (2009).
[36] J. M. Maldacena, Eternal black holes in anti-de Sitter, J. High Energy Phys. 04 (2003) 021.
[37] Y. Nakata, T. Takayanagi, Y. Taki, K. Tamaoka, and Z. Wei, New holographic generalization of entanglement entropy, Phys. Rev. D **103**, 026005 (2021).
[38] K. Narayan and Hitesh K. Saini, Notes on time entanglement and pseudo-entropy, arXiv:2303.01307.
[39] A. Lewkowycz and J. Maldacena, Generalized gravitational entropy, J. High Energy Phys. 08 (2013) 090.